Available online at www.sciencedirect.com
SCIENCE DIRECT®
Journal of Solid State Chemistry 173 (2003) 189–195
JOURNAL OF SOLID STATE CHEMISTRY
http://elsevier.com/locate/jssc

Neutron powder diffraction study of strain and crystallite size in mechanically alloyed PbTe

N. Bouad,[a] L. Chapon,[b,*] R.-M. Marin-Ayral,[a] F. Bouree-Vigneron,[c] and J.-C. Tedenac[a]

[a] *LPMC, UMR 5617 CNRS, Université Montpellier II, 5 place Eugène Bataillon, 34095 Montpellier Cédex 05, France*
[b] *ISIS Department, Bldg R3, Rutherford Appleton Laboratory, Chilton, Didcot, OX11 0QX, UK*
[c] *Laboratoire Léon Brillouin, CEA-Saclay, 91191 Gif-sur-Yvettte Cédex, France*

Received 6 August 2002; received in revised form 11 November 2002; accepted 26 November 2002

Abstract

We report on an analysis of strain and crystallite size effects in mechanically alloyed PbTe. The evolution of the microstructure was monitored by Rietveld refinements of the neutron powder diffraction data collected at room temperature. For milling times shorter than 6 h, the synthesis is not completed and the samples are clearly multi-phase with high concentrations of unreacted starting constituents. For longer milling times, the diffraction patterns are consistent with a single-phase PbTe. Within the range of reaction times studied, the crystallite size decreases with an exponential decay law and saturates to a value of 26 nm. However, the strain parameter does not show such a monotonic behavior. Indeed, it first increases and reaches a maximum when the synthesis is achieved and then drops for longer milling time as a result of the thermal activated annealing induced by additional mechanical shocks.

Keywords: Thermoelectricity; Neutron diffraction; PbTe; Microstructural effects

1. Introduction

A thermoelectric device consists of both n- and p-type semiconductors linked by electrical and thermal junctions [1]. Its efficiency is related to the figure of merit $Z = S^2\sigma/k$ (S = Seebeck coefficient, σ = electrical resistivity and k = thermal conductivity) of each branch of the device. PbTe and its related alloys (mostly PbSnTe) have been studied for years and stand as one of the best families of thermoelectric materials for middle-range temperature applications (500–700 K) [2,3]. Their reduced figure of merit ZT (a dimensionless quantity) reaches 1, which has been the experimental limit for years in bulk semiconductors. Even if emerging materials like filled-skutterudites or clathrates are undoubtedly the next candidates in that temperature regime (e.g., $ZT = 1.5$ for $Ce_fFe_{4-x}Co_xSb_{12}$, a p-type filled-skutterudite [4]), the lack of efficient n-type materials should extend the use of lead telluride, at least in the near future.

Using bulk mechanical alloying (MA) to synthesize thermoelectric materials is mainly motivated by a considerable reduction of the cost for industry, while this process is easier to bring into operation than standard high-temperature synthesis. It is also known that the materials produced by a powder processing route have greater mechanical strength when compared to conventional growth alloys. At least, this method usually leads to sub-micrometer crystallites and obviously modifies the physical properties of the compound. However, although the propagation of charge carriers and phonons are both affected by the geometrical limits of the crystallites, it is mostly the lowest-frequency phonons (largest mean free path), that are effectively scattered at the domain boundaries. Since the thermal conductivity at 500–700 K is dominated by the lattice contribution, the figure of merit is potentially enhanced when homogeneous low crystallite sizes are achieved.

In a previous publication [5], we reported the successful synthesis of PbTe by bulk MA together with

*Corresponding author.
E-mail addresses: l.chapon@rl.ac.uk (L. Chapon), ayral@lpmc.univ-montp2.fr (R.-M. Marin-Ayral), tedenac@lpmc.univ-montp2.fr (J.-C. Tedenac).
URL: http://www.isis.rl.ac.uk.

0022-4596/03/$ - see front matter © 2003 Elsevier Science (USA). All rights reserved.
doi:10.1016/S0022-4596(03)00017-3

the result of X-ray diffraction and scanning electron microscopy (SEM). The present paper is focussed on the MA reaction itself. As the reaction time goes on, we follow quantitatively the relative fractions of the starting constituents and the PbTe phase by Rietveld refinements of the neutron powder diffraction (NPD) data. The microstructural parameters (crystallite size and strain) are also extracted and their time dependence, gives new insights about the synthesis of PbTe under these specific experimental conditions.

2. Experimental

Granules of lead (99.999%, 3 mm diameter) and tellurium (99.999%, 3 mm diameter) were introduced in stoichiometric proportions (1:1) in a 45 mL Si_3N_4 vial. The material to ball weight ratio was kept constant at 1:2 for every synthesis. The vial was then sealed in a glove box under an argon atmosphere to prevent the powder from undergoing oxidation during milling. A planetary mill (Fristch® Pulverisette P7) was used and the angular speed fixed to 596 rpm. After a given reaction time, the milling was stopped and a large amount of powder (up to 3 g) was deducted from the vial for analysis by NPD. Five independent syntheses were performed corresponding to the reaction times of, respectively, 1, 3, 6, 12 and 31 h. We would like to mention that a unique synthesis is not suited to that type of study. Indeed, for short reaction times when the reaction is not completed, the deduction of a consequent amount of powder, perhaps inhomogeneous, would modify the composition of the batch for upcoming reaction times.

We also synthesized PbTe by a conventional solidification process in order to provide a reference sample accordingly with very little microstructural defects. Granules of lead and tellurium in the molar ratio 1:1 were placed in a quartz ampoule, then sealed under vacuum. The ampoule was successively heated to 873 K (rate of 5 K/min) and kept at this temperature for 20 h, then to 1273 K (rate of 5 K/min) for 1 h. The sample was then water quenched and annealed at 873 K for 10 days.

SEM coupled with energy dispersive X-ray analysis (EDX) was used to examine the milled powders.

Powder neutron diffraction data were recorded on the 3T2-high-resolution powder diffractometer at the Leon-Brillouin-Laboratory (LLB-CEA, France). The powder was placed in a 10 mm diameter vanadium can. The instrument is equipped with a Ge (335) monochromator, providing an incident wavelength of 1.2251 Å. Data were collected at room temperature in the range 6–125.7 (2θ) with a fixed step of 0.05° (2θ) and refined with the Rietveld method using the program Fullprof [6] and the Winplotr [7] interface. The profile function "Thompson–Cox–Hastings pseudo-Voigt" [8] was used for all refinements. Indeed, this function available in Fullprof integrating gaussian and lorentzian broadening for microsize and microstrain parameters, performs a correct convolution of the instrumental function considered as Voigtian, with the intrinsic profile function. Further details concerning the parametrization of such functions are included in the "Neutron Diffraction" section of the present paper.

Note that the choice of neutron rather than X-ray diffraction was mainly motivated by the opportunity to probe a consequent volume of the samples with the aim to extract reliable phase fractions in the multi-phase regime. The fall-off of the X-ray form factor with θ also limits the number of intense peaks with high Miller indices, therefore degrading the statistic for this type of analysis, especially in a system of high symmetry.

3. Tribochemical mechanism of the PbTe reaction

The results of the SEM analysis, are briefly summarized in this section to give the reader some basic insights into the system. A more detailed study is published elsewhere [5].

To study the mechanism of the PbTe formation, SEM was performed in back-scattered electron image modes. In the 1 h milled powder, brittle tellurium, which is powdered very quickly appeared to be embedded in the lead constituent and a characteristic laminar aspect can be seen (Fig. 1). A coalescence mechanism is predominant between the tellurium and the lead particles. Numerous small agglomerates consisting of a mixture of tellurium and lead were seen to be attached by fracture welding and appear with a cellular structure.

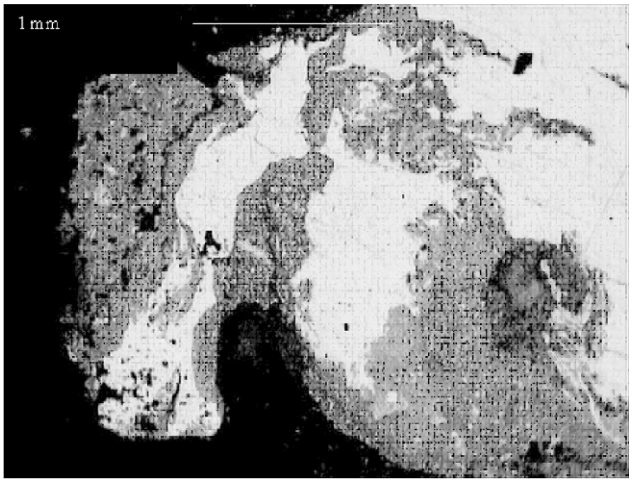

Fig. 1. SEM micrograph of the milled powder for 1 h of synthesis. The heaviest element (lead) is imaged brightly and light element (tellurium) darkly.

After 3 h of milling, there are no elemental lead and tellurium particles left: tellurium particles seem to be present as inclusions, inside lead telluride aggregates. After 6 h of milling, the powder is homogeneous and consists only of PbTe. No significant evolutions are observed for the 12 and 31 h milled powders.

4. Neutron diffraction

4.1. Standard sample

PbTe is isostructural to NaCl and crystallizes in the $Fm\bar{3}m$ space group (no. 225). Pb atoms occupy the 4(a) sites (0,0,0) while the tellurium atoms occupy the 4(b) sites $(\frac{1}{2},\frac{1}{2},\frac{1}{2})$. No impurities are detected in the neutron diffraction data and all the diffraction lines can be indexed by this space group. The result of the Rietveld refinement is plotted in Fig. 2. The refined structural parameters and the agreement factors are displayed in Table 1. We will note the excellent agreement between the structural parameters in this study and those from previous results on a single crystal [9].

For the purpose of our work, i.e., quantitative analysis of phase fractions and the extraction of microstructural parameters for the ball-milled samples, we assume at first approximation that the standard sample does not exhibit any microstructural effects. In other words, we suppose that the average crystallite size is well above 1 μm (what is usually considered to be the limit under which diffraction line broadening manifests) and that the material is free of any kind of defects (dislocations, stacking faults, microtwinning…). In such a case, the measured profile is actually the instrumental profile and, for this specific instrument, is a pure gaussian. The θ-dependence of the full-width at half-maximum (FWHM) follows the well-known empirical Caglioti formula [10]:

$$\mathrm{FWHM}^2 = U_0 \tan^2(\theta) + V_0 \tan(\theta) + W_0, \quad (1)$$

where U_0, V_0, and W_0 are refinable parameters. The values of U_0, V_0 and W_0 (see Table 1) obtained with PbTe are slightly different from the values of the intrinsic instrumental profile deduced from the measurement of Si or LaB_6. Unsurprisingly, it suggests that our standard does exhibit some weak microstructural effects. However, the difference with the intrinsic instrumental profile remains small enough to consider our model as a good starting point for other refinements. Furthermore, by choosing to do so, the reflections for the standard sample and the textured ones occur at the same scattering angle and allows a more reliable comparative study of the θ-dependence of the FWHM.

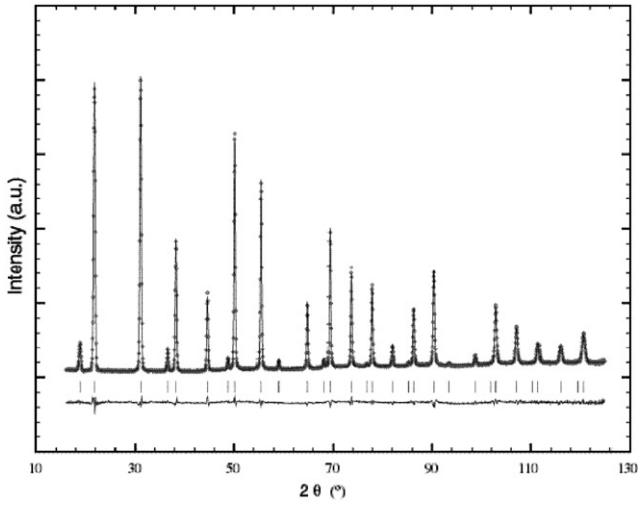

Fig. 2. Observed (◦), calculated (line) and difference (line below) plots of the Rietveld refinement for PbTe synthesized by a conventional high-temperature route. The bottom row of vertical markers indicate the angle positions of the reflections.

Table 1
Structural and profile parameters for PbTe synthesized by the conventional high-temperature route

Standard PbTe	
a (Å)	6.4611(3)
U_{Iso}(Pb) (Å^2)	0.0216(5)
U_{Iso}(Te) (Å^2)	0.0147(6)
U_0	0.319(6)
V_0	−0.417(7)
W_0	0.203(2)
R_{wp}	0.0926
χ^2	1.313
R_{F^2}	0.034

a is the lattice parameter, U_{Iso}, the isotropic thermal parameters, U_0, V_0 and W_0 are the profile parameters defined in Eq. (1). R_{wp}, R_{F^2} and χ^2 are the agreement factors of the refinement.

4.2. Textured samples

4.2.1. Quantitative analysis

The results of the Rietveld refinements for the mechanically alloyed materials are plotted in Fig. 3. Line broadening is rather visible in respect to the standard sample and indicates the onset of microstructural effects. Furthermore, new sets of reflections appear in the neutron data for samples corresponding to milling times of 1 and 3 h, suggesting the presence of additional phases. In the first case (1 h of milling), these reflections (Fig. 3a) could clearly be attributed to un-reacted Pb and Te (Pb crystallizes in the $Fm\bar{3}m$ space group with $a = 4.950$ Å the Pb atoms sitting in the 4(a) positions [11], while Te crystallizes in the $P3_121$ space group (no. 152) with the Te atoms in the 3(a) $(x,0,\frac{1}{3})$ sites [12]).

Thus, a three phases Rietveld refinement was conducted and lead to very good agreement factors, the structural parameters extracted, respectively, for the Pb and Te phases being very close to the values reported in the literature [11,12]. Interestingly, we noticed that the diffraction profile for the Te phase is much broader than for the two other phases, indicating smaller crystallite sizes and/or greater strain. Although an attempt to dissociate microstrain and sizes parameters for this latter phase failed, due to its relatively small diffraction intensities, this broadening is qualitatively in agreement with the SEM observation after 1 h of milling, i.e., the milling induces a faster powdering of Te than Pb, due to their different type of deformation (brittle for the former and plastic for the latter).

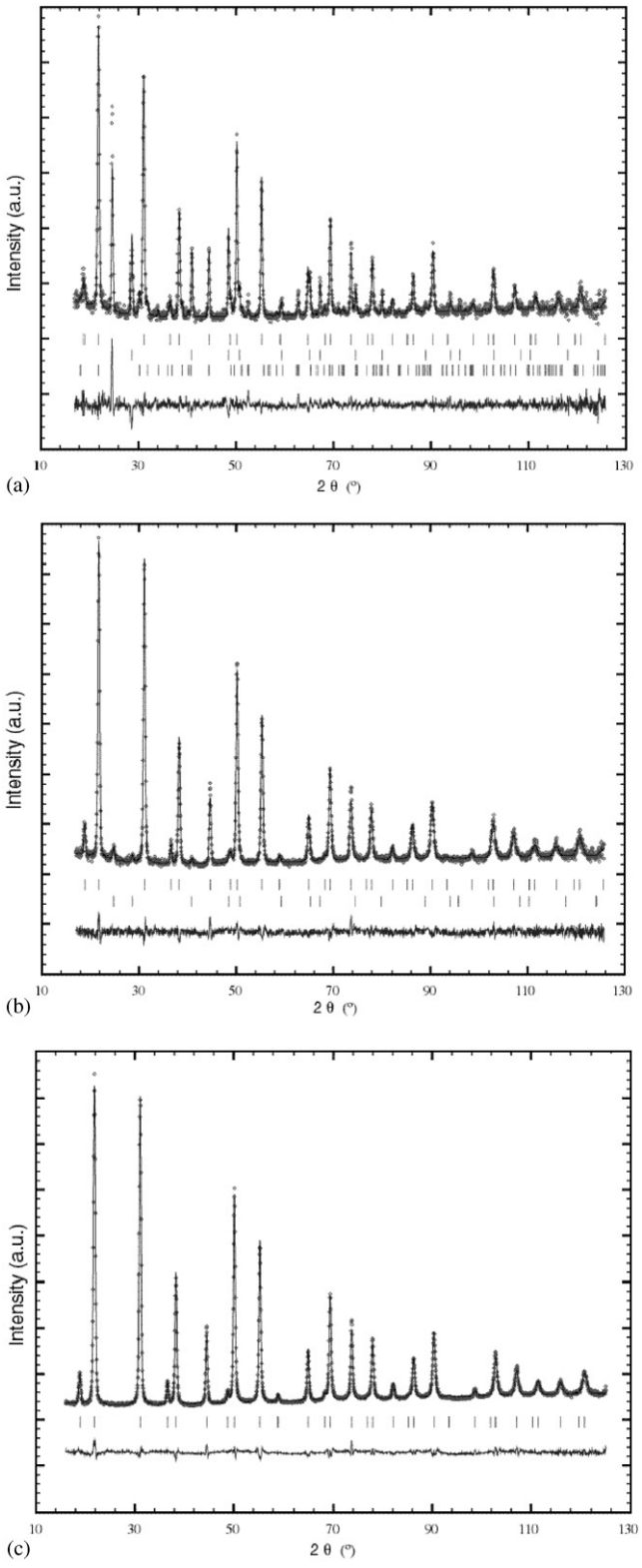

The weighted phase fractions were determined by comparison of the individual phase scale factors. After 1 h of milling time, the refined scale factors indicate the following weighted phase fractions: 62.0(1.3)% PbTe + 25.0(6)% Pb + 13.0(1.3)% Te. If we write the MA reaction with the following solid-state reaction:

$$\mathrm{Pb(s)} + \mathrm{Te(s)} \rightarrow \mathrm{PbTe(s)}, \tag{2}$$

the previous percentages indicate that the reaction is 62% completed. The molar phases fractions are thus equal to 45.3(1.3)%, 29.7(9)%, and 25.0(2.8)% i.e., taking into account the standard deviations, a similar molar amount of lead and tellurium in agreement with the writing of Eq. (2). This is also consistent with the thermodynamic phase diagram of the Pb–Te system [13] showing a very narrow range of solubility for the PbTe phase (it is almost a line compound), that forbids significant deviations from the 1:1 stoichiometry. A confirmation of this last point is provided by the refinement of the site occupancies (SOs) of Pb and Te, the ratio SO(Pb)/SO(Te) converging to 1.01. Two main phases are detected in the neutron data after 3 h of milling, Pb and PbTe (Fig. 3b). However, a careful inspection shows that the Te phase is still present but only diffuse peaks appear in the pattern with intensities just above the background. Although adding this phase to the refinement does improve the agreement factors, a strong correlation between the structural and the background parameters occurs, giving unsatisfactory results. We thus did not consider this phase and a two phases refinement was performed instead. The analysis shows that 97% of the starting constituents have reacted after 3 h.

Fig. 3. (a) Observed (◦), calculated (line) and difference (line below) plots of the Rietveld refinement for MA PbTe after 1 h of grinding operations. The vertical markers refer, respectively, to the reflection positions of the PbTe phase (upper line), Pb phase (middle line) and Te phase (lower line). (b) Observed (◦), calculated (line) and difference (line below) plots of the Rietveld refinement for MA PbTe after 3 h of grinding operations. The vertical markers refer, respectively, to the reflection positions of the PbTe phase (upper line) and the Pb phase (lower line). (c) Observed (◦), calculated (line) and difference (line below) plots of the Rietveld refinement for MA PbTe after 12 h of grinding operations.

For milling times of 6, 12 (Fig. 3c) and 31 h, all the Bragg peaks in the neutron pattern were indexed with a single-phase: PbTe, giving evidence that reaction (2) is completed within the accuracy of the experiment (usually 1% of impurity is detectable with neutron diffraction). Furthermore, it is unlikely that a large amount of amorphous starting elements is still present in the batch and the SEM images do not show evidence for it. In the neutron data, the contribution from one or several amorphous phases will give rise to a structured background. It might actually be the case in Fig. 3b) (sample $t = 1$ h), where a broad modulation around $70°–2\theta$ appears in the background, as well as an inflection at low scattering angles. However, this feature progressively disappears for longer milling time and the nearly linear variation of the background found in the standard sample is recovered for the samples corresponding to milling times greater than 3 h. The reaction is thus considered as completed for $t \geqslant 6$ h.

At least, we will notice a discrepancy between the SEM and the neutron work. For the 3 h milled powder, SEM images show a homogeneous distribution of PbTe grains, while the neutron data suggest that a few percents of Pb and Te have not yet reacted. The main reason for this discrepancy is that SEM acts as a local probe, and only narrow domains of the powder surface are examined. In spite of our efforts to repeat the measurement in different locations of the sample, SEM observations failed to locate such a small amount of impurities. Therefore, comparing the results of both techniques does not reveal inconsistencies but indicates that this work strongly benefits from the use of a macroscopic probe like neutron diffraction.

4.2.2. *Microstructural parameters*

Turning now on the analysis of the microstructural parameters, a simple observation of the neutron diffraction patterns for the milled sample show that the peak broadening evolves with milling time. A Williamson–Hall plot of the data at $t = 31$ h was performed and indicates that size and strain effects coexist. In order to dissociate the two in the Rietveld refinements, we assumed the following:

- based on the high structure symmetry and the examination of the Williamson–Hall plot, both strain and size parameters are isotropic (no (h,k,l) dependent.)
- in that case, the contribution of the size parameter to the profile follows the Scherrer formula ($1/\cos(\theta)$-dependence) while the strain parameter contributes to the profile with a $\tan(\theta)$-dependence. Then the dependencies of the gaussian (G) and lorentzian (L) parts of the total FWHM (convolution of the instrumental and intrinsic profiles) are written:[1]

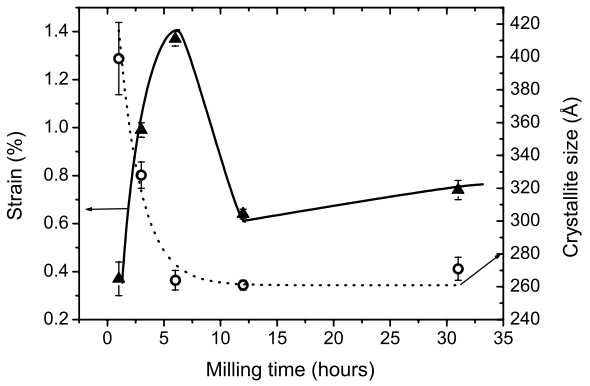

Fig. 4. Microstructural parameters vs milling time for mechanically alloyed PbTe samples. The crystallite size represents the average diameter in all directions. The solid line is a guide to the eyes (strain). The dotted line is a fit of the crystallite size with a first-order exponential decay law.

$$\mathrm{FWHM}^2(G) = U\tan^2(\theta) + V_0\tan(\theta) + W_0 + \mathrm{IG}/\cos^2(\theta),$$

$$\mathrm{FWHM}(L) = X\tan(\theta) + Y/\cos(\theta), \quad (3)$$

where V_0 and W_0 refer to the instrumental profile and are fixed to the value refined for the standard sample, and U, X, IG, Y are new parameters. U and X (resp. IG and Y) describe the gaussian and lorentzian parts of the strain parameter (resp. size parameters). A preliminary unconstrained refinement including these four parameters, was not stable and show that both the lorentzian strain and gaussian size contributions were negligible. Consequently, in the final procedures, only the lorentzian size and gaussian strain parameters were refined, while the two other factors were fixed to 0. Finally, the strain percentage and crystallite sizes were calculated from the equations:

$$S(\%) = (\pi/1.8)\sqrt{U - U_0},$$
$$\mathrm{Size}(\text{Å}) = (360\lambda/\pi^2)/Y. \quad (4)$$

Before going further, we would like to mention that the size parameter in this description represents the average diameter of the crystallite in all directions. The volume of the sphere describes the average size of the domains within which the diffraction is coherent and is expected to be much smaller than the average size of the grains (containing several crystallites). The strain percentage is representative of any defects (local disorder, stacking faults, dislocations) that increases the "stress" of a material within the

[1] A complete description of this function including anisotropic terms and a parametrization of model-dependent functions are given in the Fullprof manual, see Ref. [14].

volume defined previously and geometrically limited by the size parameter.

The evolution of size and strain parameters with milling time are plotted in Fig. 4. Clearly, one can decompose the time dependence of the microstructure in three domains:

- for times up to 6 h, the crystallite size of PbTe decreases rapidly to a value of 264(6)Å as a result of mechanical shocks induced by the milling process. At the same time, the strain increases to 1.37%. During those first 6 h, the energy provided by the milling induces the reaction (2), but also quickly generates microstructural defects.
- between 6 and 12 h, i.e., after the reaction is completed, the size of the crystallites does not change much while the strain percentage is divided by more than 2 ($S = 0.64(2)\%$). This strain relaxation is comparable to the result of a thermal annealing.
- between 12 and 31 h, neither the strain nor the size evolves (within the error bars) showing that an equilibrium is reached. The nature of this equilibrium is unclear but one may take in consideration the following: after reaction (2) is over, we first expect that the strain should increase with milling time, because the material is put under increasing stress. On the other hand, the temperature within the vial rises and it is reasonable to think that the thermal energy anneals the sample, i.e., the strain reduces. If one of these two factors dominates, the time dependence of strain would be more drastic than observed. So it seems that under the specific conditions of our synthesis, these two factors compete and give rise to a dynamic equilibrium. Of

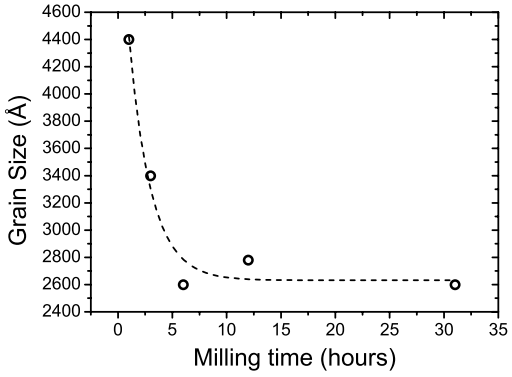

Fig. 5. Average diameter of the grains determined by BET. The dotted line is a fit of the data with a first-order exponential decay law.

Table 2
Structural, microstructural and profile parameters for PbTe synthesized by MA

Milling time (h)	1	3	6	12	31
PbTe phase					
a (Å)	6.459(1)	6.461(1)	6.461(1)	6.461(1)	6.460(1)
U_{Iso}(Pb) (Å^2)	0.024(3)	0.024(1)	0.023(1)	0.024(1)	0.024(1)
U_{Iso}(Te) (Å^2)	0.015(3)	0.016(2)	0.016(1)	0.017(1)	0.017(3)
U	0.36(1)	0.64(1)	0.93(2)	0.45(1)	0.50(1)
Y	0.112(6)	0.136(3)	0.169(4)	0.171(2)	0.165(4)
S (%)	0.37(7)	0.99(3)	1.37(3)	0.64(2)	0.74(4)
Size (Å)	399(22)	329(8)	264(6)	261(3)	271(7)
Weighted phase fraction (%)	62.0(1.3)	97.1(9)	100	100	100
R_{F^2}	0.0284	0.0336	0.0458	0.0416	0.0511
Pb phase					
a (Å)	4.950(1)	4.951(6)	—	—	—
U_{Iso}(Pb) (Å^2)	0.033(2)	0.033[a]	—	—	—
Weighted phase fraction (%)	25.0(6)	2.9(3)	0	0	0
R_{F^2}	0.152	0.217	—	—	—
Te phase					
x	0.745(8)	—	—	—	—
a (Å)	4.458(3)	—	—	—	—
c (Å)	5.925(7)	—	—	—	—
U_{Iso}(Te) (Å^2)	0.016(9)	—	—	—	—
Weighted phase fraction (%)	12.9(1.3)	—	0	0	0
R_{F^2}	0.171	—	—	—	—
R_{wp}	0.184	0.148	0.141	0.101	0.164
χ^2	1.71	1.32	1.27	1.21	1.18

a and c denote the lattice parameters (cubic for PbTe and Pb, hexagonal for Te), U_{Iso}, the isotropic thermal parameters. U and Y represent, respectively, the gaussian contribution to the strain parameter and lorentzian contribution to the size parameter defined in Eq. (3). The variable x is the refined position of the Te atoms in the Te phase (site 3(a)) R_{wp}, R_{F^2} and χ^2 are the agreement factors of the refinement.

[a] This parameters holds during the refinement.

course, the scenario we propose here is only a qualitative view and analysis under varying experimental conditions (material to ball-weighted ratio, rotation speed) must be repeated to confirm this idea.

Fig. 5 shows the result of BET Brunaner–Emmett–Teller equation (BET) measurements for the same milled samples. As BET measures the average grain size whereas powder diffraction estimates the crystallite average size, the size values determined by BET are an order of magnitude larger. Nevertheless, the trend of both curves on Figs. 4 and 5 are similar and can be fit with a first-order exponentials decay law. The ratio between grain and crystallite sizes is around 10 and almost time-independent, suggesting that hundreds of domains form within a single grain. The size of these domains (26 nm in average), is likely to be much smaller than the mean free path of acoustic phonons (for example in silicon, it was demonstrated that low-frequency phonons are characterized by a mean free path above 200–250 nm [15]), and can potentially reduce the thermal conductivity of the material. This concept leads to satisfactory results in low-dimensional structures, thin films and for example superlattices, with a major increase of the thermal conductivity in the cross-plane direction (for a review see [16]). For the same reason, our data support the idea that MA of PbTe may greatly reduce the lattice thermal conductivity of the material and is of potential interest for upcoming research on thermoelectrics (see Table 2).

5. Conclusion

The neutron powder diffraction study of mechanically alloyed PbTe samples bring new insights about the mechanism of the reaction and the evolution of the microstructural factors with milling time. During the first 6 h of grinding, the elemental constituents react and the weighted phase fraction of PbTe gradually increases to 100% at a time when the crystallite average size quickly reduces and the strain in the material increases. For longer milling times, no changes are observed on a macroscopic scale nor in the average size of the crystallites that stabilizes to 26(1) nm. However, strain is relaxed in the material after completion of the reaction and drops to half the value it was at $t = 6$ h, eventually stabilizing after 12 h. We propose that the equilibrium reached is dynamic in origin and arises from a competition between the annealing (due to a rising of the temperature within the vial) and the increasing stress produced by mechanical shocks.

We emphasize here that the grinding process, at least in the experimental conditions reported here, leads to domain sizes that are potentially small enough to affect the thermal property of the material. Further investigations of the physical properties need to be done to address this particular issue.

References

[1] D.M. Rowe, C.M. Bandhari, Modern Thermoelectrics, Holt, Rinehart & Winston, London, 1983.
[2] V. Fano, in: D.M. Rowe (Ed.), CRC Handbook of Thermoelectrics 1995, CRC, Boca Raton, pp. 257–266.
[3] D.M. Rowe, C.M. Bandhari, A review of lead telluride technology at Uwist, in: Proceedings of the Sixth International Conference on Thermoelectric Energy Conversion, University of Texas, 1986, pp. 43–54.
[4] B.C. Sales, D. Mandrus, B.C. Chakoumakos, V. Keppens, J.R. Thompson, Phys. Rev. B 23 (1997) 15081–15089.
[5] N. Bouad, R.-M. Marin-Ayral, J.C. Tedenac, J. Alloys Compd. 297 (2000) 312–318.
[6] J. Rodriguez-Carvajal, Fullprof, Version 3.5d, Oct98-LLB-JRC.
[7] T. Roisnel, J. Rodriguez-Carvajal, Winplotr Version, June 2001.
[8] R.B. Snyder, The Rietveld Method, Oxford University Press, Oxford, 1993, pp. 113–131.
[9] A.M. Reti, A.K. Jena, M.B. Bever, Trans. Metall. Soc. AIME 242 (1968) 371–373.
[10] G. Caglioti, A. Paleoti, F.P. Ricci, Nucl. Instrum. Methods 3 (1958) 223–226.
[11] H.E. Swanson, Natl. Bur. Standard. US circ 539, Vol. 1 1953, p. 34.
[12] H. McMurdie, et al., Powder diffr. 1 (1986) 76.
[13] J.C. Lin, K.-C. Hsieh, R.C. Sharma, Y.A. Chang, Bull. Alloys Phase Diagrams 10 (4) (1989) 340–347.
[14] http://www-llb.cea.fr/fullweb/fp2k/fp2k.htm.
[15] G. Chen, Phys. Rev. B 57 (1998) 14958–14973.
[16] G. Chen, M.S. Dresselhaus, J.-P. Fleurial, T. Caillat, Recent developments in thermoelectric materials, Int. Mater. Rev., to appear.